Interface of Nanoparticle-Coated Electropolished Stents

Anne Neumeister,[†] Daniel Bartke,[‡] Niko Bärsch,[‡] Tobias Weingärtner,[§] Laure Guetaz,[∥] Alexandre Montani,[∥] Giuseppe Compagnini,[⊥] and Stephan Barcikowski*[,†,#]

[†]Laser Zentrum Hannover e.V., Hollerithallee 8, 30419 Hannover, Germany

[‡]Particular GmbH, Hollerithallee 8, 30419 Hannover, Germany

[§]Institute for Applied Materials Applied Materials Physics (IAM AWP), Karlsruhe Institute of Technology (KIT), Herrmann von Helmholtz Platz 1, Building 688, 76344 Eggenstein Leopoldshafen, Germany

[∥]CEA, LITEN, DEHT LCPEM, 17 rue des Martyrs, 38054 Grenoble Cedex 9, France

[⊥]Dipartimento di Scienze Chimiche, Università di Catania, Viale A.Doria 6, Catania 95125, Italy

[#]Technical Chemistry I and Center for Nanointegration Duisburg Essen CENIDE, University of Duisburg Essen, Universitaetsstr. 7, 45141 Essen, Germany

● *Supporting Information*

ABSTRACT: Nanostructures entail a high potential for improving implant surfaces, for instance, in stent applications. The electrophoretic deposition of laser generated colloidal nanoparticles is an appropriate tool for creating large area nanostructures on surfaces. Until now, the bonding and characteristics of the interface between deposited nanoparticles and the substrate surface has not been known. It is investigated using X ray photoelectron spectroscopy, Auger electron spectroscopy, and transmission electron microscopy, for example, an electropolished NiTi stent surface and laser generated Au and Ti nanoparticles. The deposition of elemental Au and Ti nanoparticles is observed on the total 3D surface. Ti coated samples are composed of Ti oxide and Ti carbide because of nanoparticle fabrication and the coating process carried out in 2 propanol. The interface between nanoparticles and the electropolished surface consists of a smooth, monotone elemental depth profile. The interface depth is higher for the Ti nanoparticle coating than for the Au nanoparticle coating. This smooth depth gradient of Ti across the coating−substrate intersection and the thicker interface layer indicate the hard bonding of Ti based nanoparticles on the surface. Accordingly, electron microscopy reveals nanoparticles adsorbed on the surface without any sorption blocking intermediate layer. The physicomechanical stability of the bond may benefit from such smooth depth gradients and direct, ligand free contact. This would potentially increase the coating stability during stent application.

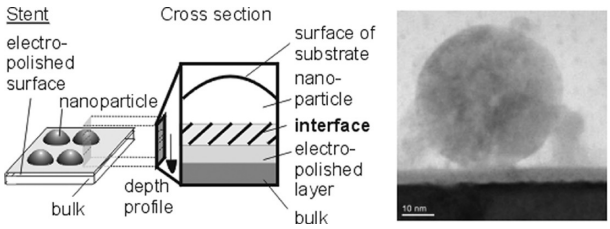

■ INTRODUCTION

Nickel−titanium (NiTi) is an outstanding material for biomedical applications, for instance, in stents used for cardiovascular applications.[1−3] The finishing process of commercial NiTi stents is mostly electropolishing and provides a protective oxide film on the surface based on titanium oxide (TiO_2).[4] However, stents with smooth surfaces are known to cause risks in terms of long term restenosis or thrombosis mainly induced by the extensive growth of smooth muscle cells, in particular, in the inner part of the stent.[5] In contrast to smooth surfaces, nanostructured surfaces entail an enhancement of endothelian cells compared to competitive smooth muscle cell growth,[6] having the potential to minimize the risk for stent application. In addition, nanostructured metal surfaces are known to influence bacterial growth and protein adsorption,[7−9] thus gaining increased interest with respect to biomedical applications.

One way to produce nanostructures is to deposit nanoparticles on surfaces using electrophoretic deposition. When voltage is applied through two electrodes, charged nanoparticles are moved in the direction of the electric field, which is developed perpendicular to the electrodes.[10] Using the implant as an electrode realizes the deposition of particles on the implant surface.[11] As an alternative to other coating procedures such as spin coating or dip coating, electrodeposition methods may be easily used for coatings of microstructures and different geometries such as round or hidden structures,[12] which is necessary in the case of stents where the inner structure is the region of interest for preventing restenosis. This method is easily implemented for nanoparticles such as ZnO, Au, Pt, and PtIr generated during laser ablation in liquids because colloidal nanoparticles generated by this method are charged.[13−15] Furthermore, laser ablation in liquids enables the generation of ligand free nanoparticles consisting of a variety of materials

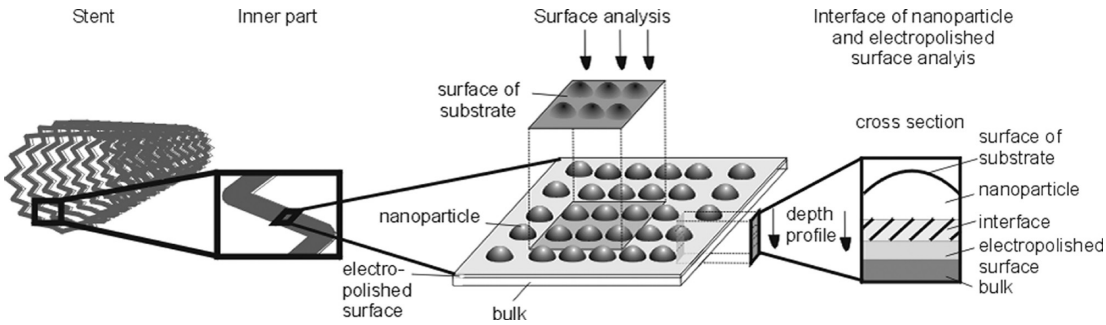

Figure 1. Schematic image of the areas and cross sections of detection for surface analysis and nanoparticle implant interface analysis.

dispersed in aqueous or organic liquids.[16−19] The electrophoretic deposition of laser generated nanoparticles has already been demonstrated on surfaces made of Au, PtIr, or NiTi.[11,14,18] Nanoparticle formation on the surface is controllable via the applied electric field, the size and concentration of the nanoparticles, and the time of deposition.[15,10]

Because nanoparticles are considered to cause adverse effects in cells, it is of major concern to prevent an unintended release of nanoparticles from substrates inserted into the body. Therefore, the interface between nanoparticles and the surface is essential to investigate. To the best of our knowledge, neither the interface between nanoparticles and the surface nor the change in the composition of the bulk material due to the coating procedure has yet to be investigated when laser generated nanoparticles are deposited via electrophoresis on substrates. An evaluation of the quality of the coating is necessary as the first step before a detailed examination of the effect on the biosystem can be performed. To preserve the conditions of a stent even after a coating has been applied, deposited nanoparticles have, at best, the same material composition as the stent substrate.

We therefore intend to investigate the surface and the interface of laser generated Ti and Au nanoparticles deposited on a NiTi electropolished surface using scanning electron microscopy (SEM), Auger electron spectroscopy (AES), X ray photoelectron spectroscopy (XPS), and transmission electron microscopy (TEM). For TEM observations, cross sectional samples were prepared using a focused ion beam (FIB), and the nanoparticle crystal structure was analyzed by X ray diffraction (XRD).

■ MATERIALS AND METHODS

Nanoparticle Generation and Electrophoretic Deposition. Nanoparticles were generated during laser ablation in 2 propanol. Ti and Au targets (Goodfellow, 99.9% purity) were irradiated using a picosecond laser system (Trumpf TruMicro 5050) delivering 7 ps pulses at 50 or 33.3 kHz (Ti or Au ablation, respectively), a wavelength of 1030 nm, and a pulse energy of 250 μJ (more details available in the Supporting Information). The process duration was 6 (Ti) and 3 min (Au), the resulting colloidal Ti nanoparticle concentration was 65 mg L^{-1}, and the Au nanoparticle concentration was 110 mg L^{-1}.

Ti nanoparticles had an average hydrodynamic diameter of 85 nm, and Au nanoparticles had an average hydrodynamic diameter of 25 nm. The zeta potentials were −45 ± 10 mV (Ti) and −30 ± 5 mV (Au).

A commercial stent (Admedes Schuessler GmbH) with an electropolished surface was used. The $Ni_{50}Ti_{50}$ stent material was used as an electrode and was dipped into the colloidal solution. The applied ac voltage was 30 V for 12.5 min for Ti nanoparticles and 7.5 min for Au nanoparticles. The electrodes were spaced 0.3 cm apart, and the applied electric field was therefore 100 V cm^{-1}.

For the NiTi reference material, the process was carried out under the same conditions in 2 propanol but without nanoparticles.

Characterization. Scanning electron microscopy was carried out using an FEG (field emission gun) SEM FEI (Quanta 400).

Auger electron spectroscopy (AES) analyses were performed with a Physical Electronics PHI 680 field emission scanning Auger nanoprobe. The depth profiles were carried out in areas with dimensions of 1 μm × 1 μm (uncoated surface), 70 nm × 70 nm (Au nanoparticle coated surface), and 50 nm × 50 nm (Ti nanoparticle coated surface). The sputtering rate was 10 nm min^{-1} for the SiO_2 standard.

X ray photoelectron spectra (XPS) were recorded using an Axis Ultra spectrometer. The sample chamber basic pressure was in the range of 10^{-9} Torr. All of the acquisition conditions were set to obtain a spectral resolution of <1 eV and a lateral resolution of 100 μm.

For TEM analyses, cross sectional samples were prepared using a focused ion beam (FIB). To avoid surface erosion during FIB milling, the nanoparticles were embedded in a protective layer. This layer consisted of the superposition of around a 100 nm thick carbon layer (surrounding the nanoparticles) and a 100 nm thick tungsten layer. The Au nanoparticles were observed in high resolution TEM (HRTEM) mode using a JEOL 3010 microscope operating at 300 kV and having a 0.17 nm Scherzer resolution. The Ti nanoparticles were observed in scanning transmission electron microscopy (STEM) imaging mode. These observations were performed on an FEI Titan microscope equipped with a Cs probe corrector.

X ray diffraction (XRD) of the dried Ti nanoparticle colloids was performed on a D8 Advance Bruker diffractometer with Cu Kα radiation (λ = 0.154187 nm). The crystallite size of the phases and their weight percentages were determined using the TOPAS 4.2 Rietveld refinement program package from Bruker.

■ RESULTS AND DISCUSSION

The strategy of the investigation is shown schematically in Figure 1. The first section of the results presents the change in the total surface characteristic due to the electrophoretic deposition of nanoparticles in comparison to that of an uncoated electropolished surface. Second, only the nanoparticle composition is characterized. The third section combines nanoparticle and surface characteristics in analyzing the interface between individual nanoparticles and an electropolished surface in terms of depth profiles as schematically drawn in Figure 1 and is abbreviated in the following text as only an interface.

Surface Analysis: Morphology and Surface Chemistry. Across the whole electropolished NiTi surface, Ti and Au nanoparticles are deposited homogenously as depicted in Figure 2 with the given parameters. Nanoparticles are deposited as one layer on the surface with interspatial distances. The surface atoms of laser generated and ligand free nanoparticles are positively charged as Muto et al. and Sylvestre et al. showed

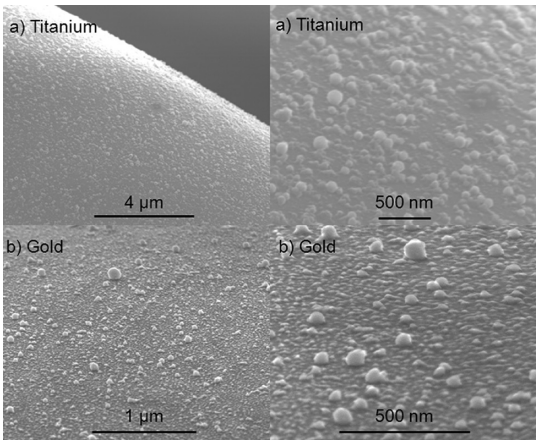

Figure 2. SEM pictures of electropolished NiTi surface with deposited laser generated (a) Ti and (b) Au nanoparticles.

for gold nanoparticles.[20,21] These particles are covered with a negatively charged Stern layer to overcompensate for the positive charge of the nanoparticle surface. This outer layer results in the negative charge of the zeta potential constructed by different charges as recently sketched by Wagener et al.[22] This negative charge on the outer layer enables electrophoresis and deposition. The deposition density depends on the applied potential, among other parameters, as He et al. reported,[23] the deposition time, and the carrier fluid.[15] (SEM images showing nanoparticle depositions using different deposition times and voltages are presented in the Supporting Information.) Thus, the 100 V cm^{-1} electric field results in a deposition characteristic that enables the examination of the interface because of identifiable isolated nanoparticles.

A relatively broad size distribution of nanoparticles ranging from 5 to 100 nm is detected on the surface. Broad, bimodal size distributions are often observed for colloidal laser generated nanoparticles,[24,25] which corresponds to what is observed in the SEM images. It is still under debate how nanoparticles are formed when generated during laser ablation in liquid. First, laser ablation causes a cavitation bubble with a lifetime of around 200 μs, as Tsuji et al. have shown, assuming that "the generation of nanoparticles would thereby mainly occur in the cavitation bubbles".[26] Generally, after the nucleation of ligand free particles within the laser induced cavitation bubble, the nanoparticles are released into the liquid after the collapse of the bubble (and some fraction may also be released during cavitation). As Sajti et al. have shown, these colloidal particles can grow on the time scale of milliseconds to seconds after formation.[27]

The composition of the surface coated with nanoparticles is investigated using XPS over a total surface area of 100 μm × 100 μm. Spectra are reported in Figure 3a and show characteristic peaks of Ti oxide in all samples with the relative spin orbit splitting ($2p_{1/2}$, $2p_{3/2}$). Because the nanoparticles are deposited with some spacing, Ti oxide mainly results from the electropolished NiTi surface. In addition to the Ti oxide, the characteristic peak of elemental Ti is also identified on the surface coated with laser generated Ti nanoparticles. The laser generated nanoparticles therefore consist solely of either elemental Ti or a mixture of TiO_2 and elemental Ti. This will be investigated in more detail in the following text.

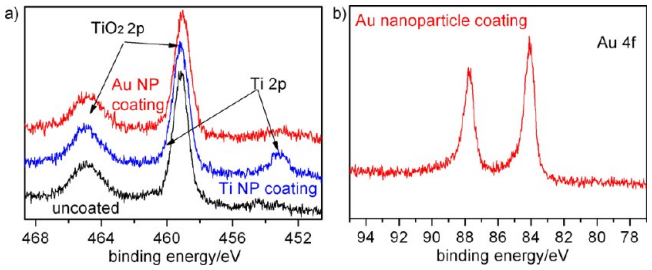

Figure 3. XPS data of an uncoated surface and surfaces with deposited Au and Ti nanoparticles. (a) The positions marked by arrows correspond to the standard values of TiO_2 2p and Ti 2p for titanium oxides and elemental titanium. (b) XPS data of a Au nanoparticle coated surface with peaks at standard values of Au $4f_{5/2}$ and Au $4f_{7/2}$ for metallic gold.

The spectrum of the surface coated with Au nanoparticles in Figure 3b reveals that the nanoparticles bound to the surface consist of elemental gold.

Besides the analysis of the total surface using XPS, a closer look at individual deposited nanoparticles allows a clear separation between deposited nanoparticles and the electro polished layer, which is essential in determining the interface. Hence, AES having a higher spatial resolution than XPS was performed on the areas shown in Figure 4a. The areas of

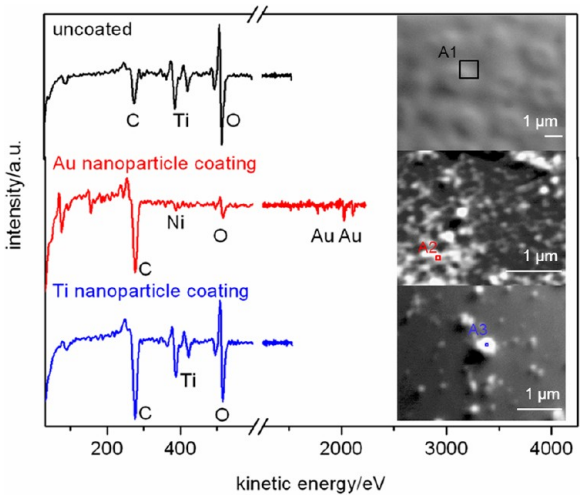

Figure 4. AES (left) and corresponding SEM images with areas of detection (right). An uncoated surface (top, spot A1), a surface coated with Au nanoparticles (middle, spot A2), and a surface coated with Ti nanoparticles (bottom, spot A3).

detection were chosen in order to exclude or minimize the signal of the uncoated surface or the background and thus to analyze solely the composition of the nanoparticles. In comparison to the coated samples, a spot on the bare surface is also investigated as a reference.

The bare surface consists mainly of oxygen, carbon, and titanium. This is in accordance with commercially electro polished NiTi stent surfaces.[28] No influence of the electro phoresis process on the surface composition is detectable.

The spectra of Au nanoparticles deposited on the surface (spot A2) clearly show the characteristic Au signal as already detected over the whole surface during XPS. The relatively large amount of carbon is probably due to the adsorption of residues from organic solvent after the generation process or

during electrophoretic deposition. It is known that a graphite shell is formed when Au nanoparticles are generated during laser ablation in toluene because of pyrolysis during the ablation process.[29] It is not known if this also occurs in 2 propanol solution. Furthermore, the SEM image of spot A2 determined a clusterlike assembly of Au nanoparticles wherein the adsorption of organic residues might be enhanced.

The spectrum from Ti nanoparticles is shown in comparison to that of the uncoated surface less oxygen. Almost half of the composition is found to be carbon. The carbon content detected in the Ti nanoparticle coating in Figure 4 is comparable to the content found in the Au nanoparticle coated sample. This indicates that the presence of carbon is independent of the elements used for nanoparticle fabrication. In fact, the detected carbon is most likely formed during the laser ablation process on the nanoparticle surface as already discussed in the case of Au nanoparticles or simply adsorbed on the electropolished surface during electrophoresis.

Overall, it could be determined that colloidal Au and Ti based nanoparticles are homogeneously deposited on the 3D surface by electrodeposition.

Interface of Nanoparticles and the Electropolished Surface: Depth Profiles. The challenge of the determination of nanoparticle bonding lies in the evaluation of the interface between nanoparticles and the stent surface. To obtain more information on this interface, AES depth profiles (schematic illustration in Figure 1) are obtained on the former analyzed areas (spots A1–A3) and are shown in Figure 5. The depth

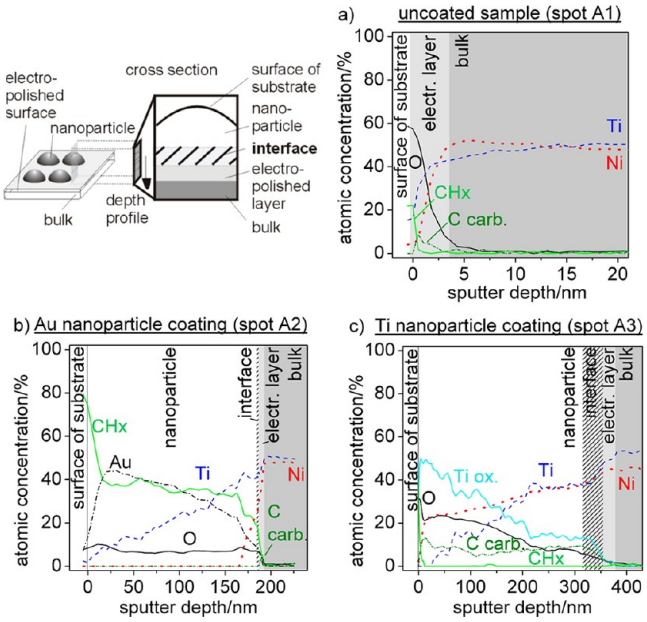

Figure 5. Sketch of the Auger depth profile and corresponding results of the (a) uncoated, (b) Au , and (c) Ti nanoparticle coated electropolished NiTi bulk.

profiles show data for the composition beginning with the surface of the substrate (in the case of a nanoparticle coating, this is attributed to the surface of the nanoparticle) and ending with the bulk composition. The interface as a region of interest lies between the nanoparticle and the electropolished layer. The gray level of the background in Figure 5 directs one to the site of the nanoparticle, interface, electropolished layer (surface of the stent), and NiTi bulk.

The uncoated sample serves as a reference, and its depth profile is shown in Figure 5a. The electropolished layer of bulk NiTi has a thickness of about 4 nm, as indicated by the oxygen, that decreases almost to zero at 5 nm depth. Accordingly, the Ni content increases until the final concentration of about 50 atom % is reached at a 5 nm depth. Hydrocarbon (CH_x) is adsorbed on the surface, and carbide bound carbon (M_xC_y) is detected as part of the electropolished layer. If carbon is present in the environment, then Ti carbide is most likely to be formed, which happens during NiTi melting procedures in carbon crucibles.[30] Hence, M_xC_y is observed in the electropolished layer.

The depth profile obtained at spot A2 on the Au coated surface (Figure 5b) detects elemental gold until a sputter depth of 180 nm is achieved. The Au content decreases constantly from 15 to 180 nm, indicating a smooth transition. However, the smooth transition might be due to ballistic recoils of Au atoms that occur during sputtering processes.[31] Interestingly, the Ti content increases constantly until its final concentration of about 50 atom % is reached at a sputter depth of 180 nm whereas the Ni content is zero until 150 nm. Further increasing depth to 180 nm shows an increase in Ni content. A high energy Ti peak was used for interpretation whereas for Ni a peak was used that lies in the low energy range. Hence, the early increase in Ti might be due to a secondary signal from the bulk material and might be higher that than for Ni.

Accordingly, at this sputter depth of 180 nm M_xC_y is also detected over a range of 5 nm, assuming that the electro polished layer is found at this depth. As noted from the AES depth profile of the uncoated surface, the electropolished layer has a depth of 5 nm. We assume that there is only a thin (<5 nm) interfacial layer between a Au nanoparticle and the electropolished layer.

Oxygen (10 atom %) and CH_x (40 atom %) are constantly detected throughout the nanoparticle until the NiTi bulk is achieved. In general, CH_x is attributed to adsorption. Furthermore, the measured depth of the deposited nano particles is 180 nm and therefore differs from the nanoparticles average size of 25 nm. This is due to a clusterlike nanoparticle structure formed in the analyzed area after electrophoretic deposition (Figure 4, SEM image). Most likely, carbon and oxygen residues originate from the organic liquid and are adsorbed in between the nanoparticles as already detected in AES of the nanoparticle surface in the previous section.

In comparison to the Au coated surface (spot A2), the Ti coated surface (spot A3) reveals only 5 atom % of carbon. Analyzed spot A3 in the Ti nanoparticle coated sample applies to one single and nearly isolated nanoparticles. No clusterlike structure with an inclusion of organic residues is observed; therefore, the carbon content is comparably low but constant. However, this constant carbon content until a sputter depth of 400 nm is reached indicates carbon formation within the nanoparticle as formed when Ti nanoparticles are generated during laser ablation in 2 propanol solution according to Golightly et al.[32] They found that during this generation process a broad composition based on Ti carbides, Ti oxides, and elemental Ti is found. To verify the observations found by Golightly et al. and to exclude Ti carbide formation occurring during the coating process, we added XRD measurements of the Ti nanoparticle colloid in 2 propanol (figure in Supporting Information). For the crystalline part of the colloid, a main cubic phase TiC (>70 wt %) and a secondary phase Ti_xO_y (<30 wt %), which probably consists of triclinic phase Ti_4O_7, were

found. The calculated average crystallite size for both phases was approximately 10−25 nm. Ti carbide is therefore formed during the nanoparticle generation process because of the presence of carbon in the organic liquid. The same elements are detected during AES of the stent surface.

The oxygen content in the nanoparticle observed in the AES depth profile is almost 25 atom % on the outer surface of the Ti nanoparticle and decreases slowly with increasing depth in relation to the decreased Ti oxide signal. Inverse to the decreasing content of Ti oxide from the nanoparticle into the bulk, the elemental Ti signal increases until 50 atom % in the bulk is achieved. The elemental Ti profile is comparable to the Ti profile already detected from a Au coated sample. In the latter, the smooth, monotonous increase in the Ti concen tration was likely due to the secondary signal from the background. This secondary signal might also result in the small increase detected in the Ti coated sample. However, this smooth interface is correlated not only to the element but also to the Ti oxide. Thus, a smooth interfacial gradient from the nanoparticle to the bulk is even more evident than in the case of Au. It is difficult to separate the phase boundaries of the nanoparticle, interface, and electropolished layer clearly because all components are found to consist of the same elements. However, by focusing on the variation of the element composition with increasing depth, we can estimate the interfacial layer thickness to be approximately 30 nm. This is $^{1}/_{10}$ of the total nanoparticle thickness where the diffusion of atoms takes place and provokes the smooth gradient obtained in the depth profiles. This layer is thicker and the gradient is even smoother in the Ti nanoparticle coated NiTi stent than in the stent with the Au nanoparticle coating.

Cross sectioned thin samples with nanoparticles deposited on the support were cut perpendicular to the surface plane using FIB and then analyzed by TEM. The TEM images (Figure 6) show the Au and Ti nanoparticles embedded in the FIB protected layers. The dark area on the bottom of the images represents the NiTi bulk. On top of the bulk, the electropolished layer with the deposited nanoparticles is depicted. Ti and Au nanoparticles are deposited on the electropolished layer with different spatial distances. The right image shows particles at higher magnification where the electropolished layer is clearly visible on top of the bulk and in direct contact with the deposited nanoparticles. The electropolished layer is 4−6 nm thick, which confirms the results from the AES depth profile.

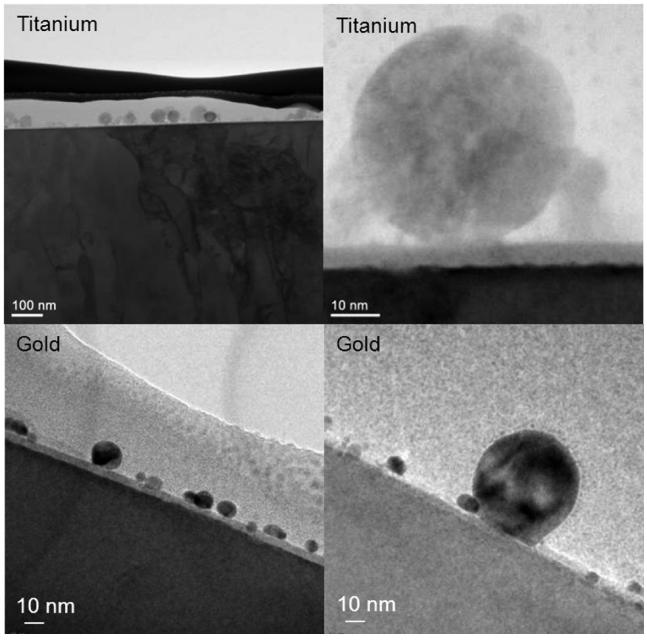

Figure 6. TEM images of the interface between deposited titanium and gold nanoparticles and the NiTi electropolished substrate.

Gold nanoparticles appear darker in the TEM pictures than does the electropolished layer because of the higher density of Au compared to that of Ti oxide. A phase boundary between the nanoparticle and the electropolished layer is visible because of the differences in the contrast. Because the AES depth profile revealed a thinner interface of the Au coated sample than of the Ti coated sample, this allowed us to assume that the Au nanoparticles are bound on the electropolished surface by physisorption. Unlike the former demonstrated AES, this spot of Au nanoparticle coating shows no clusterlike assembly.

The size in the case of the Ti nanoparticle is about 45 nm. Because the contrast of the Ti nanoparticle is similar to the contrast of the electropolished layer consisting of Ti oxide, it is most likely that the nanoparticles also consist, to a certain extent, of Ti carbide and Ti oxide, causing a smooth elemental depth profile across the interface (XRD in Supporting Information).

For all nanoparticle coatings investigated, no spacing between the nanoparticle and the implant surface is observed. It is known that laser generated and ligand free nanoparticles adsorb more efficiently on a surface than do nanoparticles stabilized with ligands.[22] Obviously, because the nanoparticles are prepared by laser ablation without using ligands or surfactants, no soft matter ligands are detected at the phase boundary of the hard matter nanoparticle coating and electro polished NiTi.

■ CONCLUSIONS

In this work, we showed that the electrophoretic deposition of laser generated colloidal nanoparticles is a suitable method for obtaining nanostructured surfaces based on Au and Ti nanoparticles deposited on 3D electropolished NiTi surfaces.

The Au nanoparticle coating causes higher amounts of adsorbed carbon and oxygen detected mainly in between the nanoparticle clusters. These residues originate from the coating process and adsorb on the surface, which needs to be considered for potential biological side effects, in particular when clusterlike structures from nanoparticles are deposited. Au nanoparticles seem to be physisorbed on the surface with the direct contact of Au nanoparticles and the electropolished surface. To decrease the formation of organic residues, nanoparticles free of soft matter ligands should be deposited on the surface. Cross sections of the phase boundary proved direct hard binding of the inorganic nanoparticle to the inorganic implant surface without intermediate organic layers.

The nanoparticle−substrate interface has also been analyzed for Ti nanoparticle coated implants in detail. Because the composition of the coating and substrate is dominated by the same element (titanium), a clear statement of the bonding of the nanoparticles by elemental analytics is difficult to make, but we have shown that there is a smooth, monotonous gradient of the elemental depth profile from the nanoparticle toward the bulk. This indicates the direct bonding of Ti based nano particles on the electropolished surface and leads to the assumption that diffusion processes at this interface take place

to a certain extent. The total surface coated with Ti nanoparticles consists of elemental Ti, Ti oxide, and Ti carbide. In terms of stent application, the nanostructured surface has an almost unaffected chemical composition compared to that of the commercial electropolished surface. It is advantageous to have the same material composition in contact with the biological environment as the surface of already certified stent materials, with only nanotopography being modified. Additionally, a sufficient bonding of nanoparticles and the substrate would prevent an unintended release of nanoparticles. Moreover, colloidal laser generated nanoparticles are known to dissolve in culture media up to 15%.[33] Therefore, the risk of dissolution of nanoparticles when deposited on the substrate surface is even lower.

We characterized the interface between electrodeposited nanoparticles and the electropolished NiTi surface for the first time as having the potential to fabricate nanoparticle coatings with smooth, monotonous elemental gradients. Such coatings made of Ti based nanoparticles on Ti based substrate surfaces are free of intermediate (soft matter) layers and may have improved physicomechanical stability compared to that of nanoparticle coatings made of different elements or with intermediate bonding layers. Hence, Ti based nanoparticle coatings may be a route to fabricating physicomechanically stable nanostructure modified stents.

In the future, the bioresponse of such coatings will have to be tested to validate our physicochemical findings on the nanoparticle–stent interface. Additionally, the mechanical stability of the nanoparticle coating before and after the insertion of stents needs to be evaluated. For example, as presented by Eppler et al. and Riboh et al., measuring nanoparticle adhesion (or the adhesion force) affords a sophisticated method of development[34,35] that needs to be established for the demonstrated coating.

■ ASSOCIATED CONTENT

● Supporting Information

Further experimental data including scanning electron micro graphs, nanoparticle size distribution, XRD data, and detailed information on the experiments. This material is available free of charge via the Internet at http://pubs.acs.org.

■ AUTHOR INFORMATION

Notes

The authors declare no competing financial interest.

■ ACKNOWLEDGMENTS

We thank the European Commission for founding parts of the analysis within EUMINAfab. This work was partially carried out with the support of the Karlsruhe Nano Micro Facility (KNMF), a Helmholtz Research Infrastructure at Karlsruhe Institute of Technology (KIT). We acknowledge the German Research Foundation for funding parts of this work within the Collaborative Research Centre TransRegio 37 Micro and Nanosystems in Medicine – Reconstruction of Biologic Functions and within the excellence cluster REBIRTH. In particular, GmbH acknowledges its financial support by the German Federal Ministry of Economics and Technology (BMWi) within the program EXIST Transfer of Research. We are also grateful to Dr. Oleg Prymak from the Department for X ray Diffraction of the Institute of Inorganic Chemistry, University of Duisburg Essen, for the measurement and the following evaluation of the results and helpful discussions.

■ REFERENCES

(1) Morgan, N. B. Medical shape memory alloy applications–the market and its products. *Mater. Sci. Eng. A* **2004**, *378*, 16–23.

(2) Yahia, L. H. Shape memory implants in medicine: orthopaedics, dental and cardiovascular applications. *Arch. Physiol. Biochem.* **2000**, *108*, 121.

(3) Kapila, S.; Sachdeva, R. Mechanical properties and clinical applications of orthodontic wires. *Am. J. Orthod. Dentofacial Orthop.* **1989**, *96*, 100–109.

(4) Stoeckel, D.; Pelton, A.; Duerig, T. Self expanding nitinol stents: material and design considerations. *Eur. Radiol.* **2004**, *14*, 292–301.

(5) Bennett, M. R.; O'Sullivan, M. Mechanisms of angioplasty and stent restenosis: implications for design of rational therapy. *Pharmacol. Therapeut.* **2001**, *91*, 149–166.

(6) Choudhary, S.; Haberstroh, K.; Webster, T. J. Enhanced functions of vascular cells on nanostructured Ti for improved stent applications. *Tissue Eng.* **2007**, *13*, 1421–1430.

(7) Elter, P.; Lange, R.; Beck, U. Electrostatic and dispersion interactions during protein adsorption on topographic nanostructures. *Langmuir* **2011**, *27*, 8767–8775.

(8) Diaz, C.; Schilardi, P. L.; Salvarezza, R. C.; Fernandez Lorenzo de Mele, M. Nano/microscale order affects the early stages of biofilm formation on metal surfaces. *Langmuir* **2007**, *23*, 11206–11210.

(9) Emerson, R. J.; Bergstrom, T. S.; Liu, Y.; Soto, E. R.; Brown, C. A.; Grant McGimpsey, W.; Camesano, T. A. Microscale correlation between surface chemistry, texture, and the adhesive strength of *Staphylococcusepidermidis*. *Langmuir* **2006**, *22*, 11311–11321.

(10) Biest, O.O. Van d.; Vandeperre, L. J. Electrophoretic deposition of materials. *Annu. Rev. Mater. Sci.* **1999**, *29*, 327–352.

(11) Jakobi, J.; Menendez Manjon, A.; Chakravadhanula, V. S. K.; Kienle, L.; Wagener, P.; Barcikowski, S. Stoichiometry of alloy nanoparticles from laser ablation of PtIr in acetone and their electrophoretic deposition on PtIr electrodes. *Nanotechnology* **2011**, *22*, 145601–145608.

(12) Dickerson, J. H., Boccaccini, A. R., Eds. *Electrophoretic Deposition of Nanomaterials*; Springer: New York, 2012.

(13) Tsuji, J. S.; Maynard, A. D.; Howard, P. C.; James, J. T.; Lam, C.; Warheit, D. B.; Santamaria, A. B. Research strategies for safety evaluation of nanomaterials, part IV: risk assessment of nanoparticles. *Toxicol. Sci.* **2006**, *89*, 42–50.

(14) Menendez Manjon, A.; Chichkov, B. M.; Barcikowski, S. Influence of water temperature on the hydrodynamic diameter of gold nanoparticles from laser ablation. *J. Phys. Chem. C* **2010**, *114*, 2499–2504.

(15) Menendez Manjon, A.; Jakobi, J.; Schwabe, K.; Krauss, J. K.; Barcikowski, S. Mobility of nanoparticles generated by femtosecond laser ablation in liquids and its application to surface patterning. *J. Laser Micro/Nanoeng.* **2009**, *4*, 95–99.

(16) Jakobi, J.; Petersen, S.; Menendez Manjon, A.; Wagener, P.; Barcikowski, S. Magnetic alloy nanoparticles from laser ablation in cyclopentanone and their embedding into a photoresist. *Langmuir* **2010**, *26*, 6892–6897.

(17) Besner, S.; Kabashin, A. V.; Winnik, F. M.; Meunier, M. Ultrafast laser based "green" synthesis of non toxic nanoparticles in aqueous solutions. *Appl. Phys. A* **2008**, *93*, 955–959.

(18) Compagnini, G.; Scalisi, A. A.; Puglisi, O. Ablation of noble metals in liquids: a method to obtain nanoparticles in a thin polymeric film. *Phys. Chem. Chem. Phys.* **2002**, *4*, 2787–2791.

(19) Tsuji, T.; Ozono, S.; Hirai, T.; Mizuki, T.; Tsuji, M. One step preparation of superlattices and nanocrystals using laser ablation. *J. Appl. Phys.* **2009**, *106*, 054313–6.

(20) Muto, H.; Yamada, K.; Miyajima, K.; Mafune, F. Estimation of surface oxide on surfactant free gold nanoparticles laser ablated in water. *J. Phys. Chem. C* **2007**, *111*, 17221–17226.

(21) Sylvestre, J. P.; Kabashin, A. V.; Sacher, E.; Meunier, M.; Luong, H. T. Stabilization and size control of gold nanoparticles during laser ablation in aqueous cyclodextrins. *J. Am. Chem. Soc.* **2004**, *126*, 7176–7177.

(22) Wagener, P.; Schwenke, A.; Barcikowski, S. How citrate ligands affect nanoparticle adsorption to microparticle. *Langmuir* **2012**, *28*, 6132−6140.
(23) He, H.; Cai, W.; Lin, Y.; Chen, B. Surface decoration of ZnO nanorod arrays by electrophoresis in the Au colloidal solution prepared by laser ablation in water. *Langmuir* **2010**, *26*, 8925−8932.
(24) Barcikowski, S.; Hahn, A.; Kabashin, A. V.; Chichkov, B. N. Properties of nanoparticles generated during femtosecond laser machining in air and water. *J. Appl. Phys. A* **2007**, *87*, 47−55.
(25) Menendez Manjon, A.; Barcikowski, S. Hydrodynamic size distribution of gold nanoparticles controlled by repetition rate during pulsed laser ablation in water. *Appl. Surf. Sci.* **2011**, *257*, 4285−4290.
(26) Tsuji, T.; Okazaki, Y.; Tsuboi, Y.; Tsuji, M. Nanosecond time resolved observations of laser ablation of silver in water. *Jpn. J. Appl. Phys.* **2007**, *46*, 1533−1535.
(27) Sajti, C. L.; Barchanski, A.; Wagener, P.; Klein, S.; Barcikowski, S. Delay time and concentration effects during bioconjugation of nanosecond laser generated nanoparticles in a liquid flow. *J. Phys. Chem. C* **2011**, *115*, 5094−5101.
(28) Shabalovskaya, S.; Anderegg, J.; Van Humbeeck, J. Recent observations of particulates in Nitinol. *Mater. Sci. Eng. A* **2008**, *481*−*482*, 431−436.
(29) Amendola, V.; Rizzi, G. A.; Polizzi, S.; Meneghetti, M. Synthesis of gold nanoparticles by laser ablation in toluene: quenching and recovery of the surface plasmon absorption. *J. Phys. Chem. B* **2005**, *109*, 23125−23128.
(30) Frenzel, J.; Neuking, K.; Eggeler, G. Induction melting of NiTi shape memory alloys − the influence of the commercial crucible graphite on alloy quality. *Materialwiss. Werkstofftech.* **2004**, *35*, 352−358.
(31) Averback, R. S.; Ghaly, M.; Bellon, P. Interfacial effects during ion beam processing of metals. *Mater. Sci. Eng. B* **1996**, *37*, 38−48.
(32) Golightly, J. S.; Castleman, A.W. J. Analysis of titanium nanoparticles created by laser irradiation under liquid environments. *J. Phys. Chem. B* **2006**, *110*, 19979−19984.
(33) Hahn, A.; Fuhlrott, J.; Loos, A.; Barcikowski, S. Cytotoxicity and ion release of alloy nanoparticles. *J. Nanopart. Res.* **2012**, *14*, 1−10.
(34) Eppler, A. S.; Rupprechter, G.; Anderson, E. A.; Somorjai, G. A. Thermal and chemical stability and adhesion strength of Pt nanoparticle arrays supported on silica studied by transmission electron microscopy and atomic force microscopy. *J. Phys. Chem. B* **2000**, *104*, 7286−7292.
(35) Riboh, J. C.; Haes, A. J.; McFarland, A. D.; Yonzon, C. R.; Van Duyne, R. P. A nanoscale optical biosensor: real time immunoassay in physiological buffer enabled by improved nanoparticle adhesion. *J. Phys. Chem. B* **2003**, *107*, 1772−1780.